1 Parameter Space Exploration

I sometimes ponder on variation form and it seems to me it ought to be more restrained, purer.
(Johannes Brahms)

The rationale for using parameter space variation as a means to model physiological variation is presented, with caveats appropriate for this thesis given. Details of which parameters are varied are given, with reasons for their choice. An examination of the efficacy of various different commonly used biomakers as a measure of goodness-of-fit is presented, with a view to determining which biomarkers are most suited under conditions that may include experimental noise. The results of parameter variation for two separate computational model frameworks are explored, and models that reproduce experimentally observed variation are isolated, with patterns amongst the parameters that contribute to these populations being discussed.

1.1 Reproduction of Experimental Variation

As was elaborated on in §??, variation is a constant companion in the experimentalist's world. As computational models of biological processes become more complex, with advancing technology allowing us to discard earlier assumptions made for the sake of computational tractability, and further advances in experimental results allow greater understanding of the system being modelled, variation is now increasingly becoming the computational modeller's companion as well. It is to be noted that this variability includes the so-called experimental variation, the 'noise' that can get in the way of the 'true' data, but also includes the variation that is a normal, and perhaps essential, component of physiological symptoms.

However, exactly *how* this variation is to be modelled is a question left to the modeller—there are many possible alternatives. Which of these alterantives is to be used depends on the exact question being asked: what system is being modelled, how its output is being assessed, and so forth. It depends further on the available resources, and the demands being made of those resources. Were resources

and capabilities infinite and on demand, a fully stochastic, molecular model, subject to multiple simulations, would accurately and precisely model the system—indeed, for all intents and purposes, it would *be* the system. However, not only are resources finite, such a model would be drastic overkill for most research questions regarding cardiac physiology. Instead, much like the research question being posed drives the model choice, it also drives the methodology for reproduction of variability, if it is required—it should be as complex as required, but it need not be any more so.

It is the main drive of this thesis to demonstrate a method for reproducing the observed experimental variation that is

- biophysically detailed,
- computationally tractable, and
- easily scalable.

To this end, we utilise the population level approach used previously in neuron modelling (Marder and Taylor, 2011). As compared to stochastic simulations, such a methodology is computationally simpler—due to their complexity and the requirement for multiple simulations for their statistical properties to be refined, stochastic models are often limited to phenomenological, small scale models. This thus ties in to the other advantage of the model population approach: the biophysical detail that can be applied via such a process. In prescribing variation to certain biophysically specific properties, and observing the consequences, specific output variation effects can be attributed to specific input variation effects. It should be noted, however, that Heijman et al. (2013) recently demonstrated the feasibility of using a biophysically-detailed stochastic model, although it is still restricted to small-scale simulations.

Using parallelisation available by means of the Nimrod/G distributed computing grid and its various alternatives, a population model approach is also computationally tractable—each individual simulation can be computationally simple, and correct distribution can ensure that non-specialised computing resources are sufficient to the task. Finally, it is also easily scalable. By this, it is meant that not only is it a simple process to introduce variation to further parameters of interest, but also that the methodology is trivially applicable to multiple models (indeed, this thesis is based on investigations using two different models).

1.1.1 Comparison with Alternative Methods

It should be noted that the complete, multi-dimensional parameter sweep method used here provides significant benefits compared to other possible methods, insofar as the goals of this thesis are concerned. By this, it is meant that alternative methods for examining the effect of multiple parameter variation are not appropriate for this thesis. For the purposes of comparison, we may consider three alternative methods:

1. Stochastic Models (Heijman et al., 2013)
2. Multi-variable regression analysis (Sobie, 2009; Sobie and Sarkar, 2011; Sarkar and Sobie, 2010, 2011),
3. Sampling from the multi-dimensional parameter space (Britton et al., 2013),

Further details of these methods can be found in §??. It should be noted that significant work has been achieved using single parameter variation, both in deterministic studies (Romero et al., 2009, 2011) and in stochastic studies (Pueyo et al., 2011; Hashambhoy et al., 2011; Sato et al., 2009; Tanskanen et al., 2005), but this thesis is explicitly multi-dimensional in scope.

The advantages for this thesis of the population approach over stochastic approaches depends, precisely, on what stochastic approach is being used. In most cases, however, stochastic models are far less computationally tractable, especially for large simulations. This presents limits on the scale of the model that can be simulatted using stochastic means. If one applies stochasticity to multiple parameters (to provide an analogy to the goal of this thesis), the spatial scale of the simulation is curtailed (Heijman et al., 2013). It can also be noted that some studies apply stochasticity within a phenomenological model, but this prevents analysis on the biophysical source of the variability (Walmsley et al., 2010).

Multi-variable regression analysis samples from a given parameter space, and uses this to return the effect matrix $\mathbf{B}$ that approximates the effect each parameter has on a given biomarker (Sobie, 2009; Sobie and Sarkar, 2011; Sarkar and Sobie, 2010, 2011). This methodology is limited by not only sampling from a limited number of models from the total parameter sapce, but also reduces the analysis to a pseudo-single dimensional one—the entries in $\mathbf{B}$ provide insight to the effect of a single parameter on a single output, and it has been demonstrated that the overall effect is relatively accurately approximated by the linear summation of the effects. However, it provides little insight into the interactions between parameters, and especially how these interactions can vary given changes in other parameters (*i.e.* parameters X and Y are correlated in a particular manner when parameters $\{A, B, C\}$ have these values, but are correlated in a different manner when $\{A, B, C\}$ have different values).

Methodologically, the most similar method to the current is to sample from the multi-dimensional space to generate a population. This was done by (Davies et al., 2012), but only generated a population of 19 models for a canine ventricular AP. The work previously mentioned by Britton et al. (2013) presents the most comprehensive study in cardiac studies. However, sampling from the multi-dimensional space likely gives an incomplete picture, and is thus less suited to analyse the effects of multiple parameter variation. While it does present a computationally efficient means of population production, it should be noted that (a) it may be unable to give a comprehensive account of the parameter variation within the space and (b) Gemmell et al. (2010) suggests that there may be 'islands' within the population, and insufficient sampling will either miss these islands, or falsely connect them with nearby groups in the parameter space; further consideration of these problems is given in §1.4.2).

1.1.2 Caveats

It should be noted that constructing a population of models based on a single framework (replacing the initial parameter set with a parameter space) allows for a biophysically realistic method of reproducing physiological variation which remains computationally tractable. However, there are several key points that must be remembered that represent the limitations of this, and many related, approach.

1. The underlying assumptions regarding the original model still apply. As such, any inaccurate assumptions remain present in derived populations Noble and Rudy (2001); Quinn and Kohl (2013).

2. The populations derived using experimental data rely on these data remaining appropriate for the considered task. The populations used in this thesis are derived using 'healthy' data. As such, without further adaptation, the populations are unsuitable for assessing some experimental situations without appropriate alterations made to the framework, *e.g.* where cardiac remodelling has occurred (Walmsley et al., 2013).

3. Related to the point above is the fact that the model populations are united by the data used to create them. As such, if the training data used include differences such as gender, the models cannot then be used to address specific questions regarding gender—these differences are now implicitly encoded within the population.

For this dissertation, cell models are being used, but tissue data are being used for training the population. Moving from cell to tissue represents a large computational task, for two reasons. Firstly, the simple matter of simulating tissue is more computationally intensive, though preliminary simulations using the original Shannon model indicated little difference between the AP generated using cell simulations and those from tissue simulations (performed using the Chaste software (Mirams et al., 2013)). Secondly, and more pertinent for this thesis, is the problem of cell coupling (which itself is a likely candidate for variation). Heijman et al. (2013) predict that cell coupling works to reduce variation between two different cells—by this token, it is likely that any cell model population trained using tissue data is likely to represent an underestimate of the actual variation possible within a cell population. However, to exhaustively test this is computationally challenging. Consider the following: suppose it is wished to test just 20 different cells. To exhaustively examine every possible combination of this population in a 2 cell chain, it would be required to perform 20^2. It is simple to abstract this—for a possible cell population of n, in a tissue sample of size m, the number of simulations that would have to be run would be n^m. While there are many possible ways to reduce the search space, it is beyond the scope of this thesis to consider them.

Finally, there is a caveat common to almost all attempts to reproduce variation; indeed, it can be applied to most models as well. Walmsley et al. (2013) demonstrated little correlation between AP and Ca^{2+} biomarkers—this will be expanded upon in §1.5.

1.2 Construction of the Parameter Space

The computational tools involved in investigating the effects of multiple parameter variation were described in the previous chapter—the specific methods used to that end and biological reasons for these methods are described here.

Parameters describing the peak conductance for six different ion channels were varied in this study. The currents considered (with their conductance given in parentheses) were: the transient outward current (g_{to}), the rapid delayed rectifier K^+ current (g_{Kr}), the slow delayed rectifier K^+ current (g_{Ks}), the inward rectifying K^+ current (g_{K1}), the L-tpye Ca^{2+} current ($g_{\text{Ca,L}}$), and the Na^+/K^+ pump current (g_{NaK}). These currents were picked in preference to other possible choices based on their perceived impact on the repolarisation of the AP, which has been noted as an indicator of impact on beat-to-beat variability of repolarisation duration (BVR); a longer plateau implies greater BVR (Heijman et al., 2013). Furthermore, the dynamics of these currents were not changed on the basis that (a) it was expected that AP variability is primarily a result of differences in the relative magnitude of the currents rather than the dynamics, and (b) conductance is often the most poorly defined variable within

the equations defining these currents in the models. This difficulty in parameter estimation comes from both the inherent experimental difficulties in measuring peak conductance, and the variation in the experimental techniques used to define these values (with methods sometimes being poorly defined) (Quinn et al., 2011).

The conductances were varied by 0%, $\pm 15\%$, and 30%, resulting in 15,625 different models for each framework. This variation is in line with the extent of variation used in previous studies (Romero et al., 2009, 2011; Walmsley et al., 2013), and is also consistent with the range of experimentally observed variation (Fülöp et al., 2004; Iost et al., 1998; Li et al., 1999; Szentandrássy et al., 2005; Verkerk et al., 2005; Sims et al., 2008) (for further detail, see §??). While some computational studies have used greater degrees of variation, it was decided the variation applied here provided the best compromise between scale and resolution of the parameter space. Furthermore, variation of such scale is not often seen in experimental literature.

Simulations were conducted a three different cycle lengths (CLs) of 400 ms, 600 ms and 1,000 ms to constrain the population of models further—Syed et al. (2005) has demonstrated the importance of considering multiple CLs in order to accurately fit restitution curves. Furthermore, this methodology allows examination of rate-dependent effects, *e.g.* changing parameter importance, changing degrees of output variation.

1.3 Accuracy of Biomarkers in Defining Model Fit

One of the goals of this thesis is to measure the efficacy of commonly used biomarkers in assessing goodness-of-fit for populations. With a parameter sweep providing a population of models, and thus a population of data, that is free from experimental noise, this provides an opportunity for an assessment of such a question. Without having to consider the problems of experimental noise, the entire range of recorded data can be used to compare a given model output to given training data. The goodness-of-fit by this comprehensive measure can then be compared to the goodness-of-fit given by other biomarkers.

In this specific case, the NRMSD metrics defined in §?? were used to compare the output of any given model to the output of the original, unaltered model (*i.e.* the model with 0% variation for all parameters). As previously stated, M_{NRMSD} is unsuited to situations with experimental noise, but in situations where there is no computational noise (as in this parameter search), it provides a comprehensive measure of goodness-of-fit. On the assumption that, due to its involving the totality of available data, it provides the 'best' measure of goodness-of-fit, it it is then possible to assess how closely other biomarkers come to agreeing with this new gold standard; those biomarkers that come closest to defining the same models as the NRMSD metrics as 'matching' training data will then be considered accurate measures of goodness-of-fit in their own right.[1] This process uses multiple biomarkers in unison, *e.g.* APD_{50} and APD_{90}, rather than individual biomarkers in isolation.

The ~ 250 models most closely matching the original model output were determined, based on the minimum values of M_{NRMSD}. Similarly, the ~ 250 models that match original model output was determined based on minimum percentage difference according to groups of biomarkers. The degree

[1] It can be noted that, for cells with a long diastolic interval, small differences in V_{rest} would increase AP_{NRMSD} to a great degree, while the rest of the AP may provide an excellent fit to data. Fortunately, both Shannon and Mahajan populations show little variation in V_{rest}, so this problem is not realised

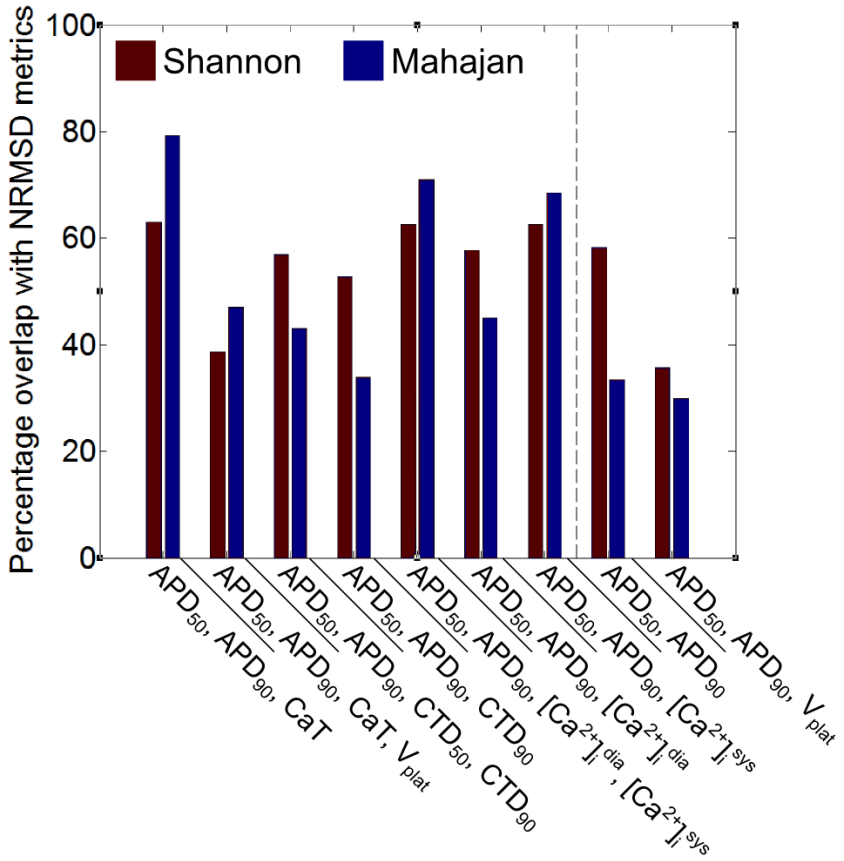

Figure 1.1: *Percentage overlap of matches between original model output and model output generated using the* ~ 250 *parameter sets determined by the NRMSD metrics ([*AP_{NRMSD} *and* $\mathrm{Ca}^{2+}_{\mathrm{NRMSD}}$*]) and by combinations of biomarkers. While all combinations of biomarkers were tested, those shown represent the combinations with the highest percentage overlap. Combinations to the left of the dashed line include information about both* V_m *and* $[Ca^{2+}]_i$*, while those to the right include only* V_m *data.*

of overlap between these two groups (those determined by NRMSD metrics and those determined by biomarkers) was then calculated.

The results of the comparison for some biomarker groups is shown in Fig. 1.1. When $[Ca^{2+}]_i$ data is available, and thus Ca^{2+} biomarkers can be used in assessing the goodness-of-fit, the accuracy (judged by percentage overlap) is increased overall. The degree of overlap for groups of metrics is not identical between the Shannon and Mahajan populations. However, overall, a combination of APD_{50}, APD_{90} and CaT (or APD_{50} and APD_{90} where $[Ca^{2+}]_i$ data are not available), is the most accurate measure of goodness-of-fit compared to NRMSD metrics. Consequently, these combinations were used for the remainder of this thesis.

Biomarker	CL (ms)		
	400	600	1,000
APD_{50} (ms)	$104 - 135$	$116 - 159$	$137 - 188$
APD_{90} (ms)	$142 - 185$	$160 - 220$	$167 - 230$

Table 1.1: *Normal range of rabbit epicardial APD_{50} and APD_{90} used to define physiological parameter sets. Values are derived from previously reported studies, as described in the text.*

Model	CL (ms)						
	400	600	1,000	400∩600	400∩1,000	600∩1,000	400∩600∩1,000
Shannon	1,691	2,631	5,352	1,384	1,511	2,526	1,352
Mahajan	3,946	1,031	0	577	0	0	0
Expanded Mahajan	9,447	11,229	5,650	6,797	779	4,331	779

Table 1.2: *Number of parameter sets producing both APD_{50} and APD_{90} values within the physiological range. Parameter values were varied by $\pm 30\%$ from the original parameter set, and then further for the Mahajan model ('Expanded Mahajan') as explained in the text. $x \cap y$ and $x \cap y \cap z$ represent parameter sets that produce physiological values at a CL of x and y, or a CL of x, y, and z, respectively.*

1.4 Defining a Population of Models to Reproduce Physiological Variation

1.4.1 Variation within the Population

In order to constrain the populations of models to those representing physiological variability, only parameter sets that produced APD_{50} and APD_{90} values that fell within the normal range for rabbit epicardium were included. APD_{90} for rabbit epicardium has been well documented and a physiological range was readily established for all CLs (Biagetti and Quinteiro, 2006; Chen et al., 2006; Eckardt et al., 1998; Goldhaber et al., 2005; Jung et al., 2011; Kirchhof et al., 2003; Kurz et al., 1993; McIntosh et al., 2000; Szigligeti et al., 1996; Wu et al., 2011; Yan et al., 2001). Reports of APD_{50} values sufficient to derive a normal range, however, were not available at all CLs. Thus, values from the literature were used to establish a mean value for APD50 (Eckardt et al., 1998; Kirchhof et al., 2003). It was then assumed that the percentage variation from mean for APD_{50} is the same as the percentage variation from mean for APD_{90}. By this assumption, an assumed range for APD_{50} that is similar to the range for APD_{90} is calculated, and used in subsequent analysis. The resulting values are shown in Table 1.1.

By using these values, it was possible to constrain the tested parameter space to a population of models that reproduces experimentally measured variability at each CL. The number of models in each population at each CL is given in Table 1.2. Those models that produce output within the physiological range are defined to be in the model population that can reproduce given variation at all CLs; the minimum, mean and maximum values of all computed biomarkers for the Shannon and Mahajan populations thus defined are shown in Table ??.

With the Shannon framework, there existed at least one parameter set that produced a physiological output at each CL, with some of these generating a physiological output at all CLs. On the other hand, while a relatively large number of models produced a physiological output at a CL of 400 ms with the Mahajan framework (the CL for which the original Mahajan model was designed), fewer

Biomarker	CL (ms)	Model	Minimum	Mean	Maximum
$(dV_m/dt)_{max}$ (Vs^{-1})	400	Shannon	233	302	329
		Mahajan	200	230	252
	1,000	Shannon	278	327	352
		Mahajan	248	279	311
V_{rest} (mV)	400	Shannon	−92	−88	−82
		Mahajan	−88	−86	−85
	1,000	Shannon	−88	−86	−81
		Mahajan	−89	−88	−87
APD_{50} (ms)	400	Shannon	112	126	135
		Mahajan	104	108	117
	1,000	Shannon	137	155	181
		Mahajan	165	182	188
APD_{90} (ms)	400	Shannon	143	154	169
		Mahajan	142	155	185
	1,000	Shannon	167	186	217
		Mahajan	207	223	230
$[Ca^{2+}]_i^{dia}$ (μM)	400	Shannon	1.24	1.29	1.32
		Mahajan	0.29	0.37	0.47
	1,000	Shannon	0.82	0.84	0.86
		Mahajan	0.15	0.16	0.18
$[Ca^{2+}]_i^{sys}$ (μM)	400	Shannon	4.49	4.92	5.22
		Mahajan	1.43	2.78	4.46
	1,000	Shannon	3.13	3.33	3.68
		Mahajan	0.41	0.59	0.76
CaT (μM)	400	Shannon	3.25	3.63	3.91
		Mahajan	1.14	2.41	4.00
	1,000	Shannon	2.30	2.49	2.82
		Mahajan	0.26	0.42	0.58
CTD_{50} (ms)	400	Shannon	123	130	134
		Mahajan	133	139	147
	1,000	Shannon	139	150	157
		Mahajan	208	231	268
CTD_{90} (ms)	400	Shannon	263	267	271
		Mahajan	245	249	260
	1,000	Shannon	382	394	404
		Mahajan	460	510	585

Table 1.3: *Minimum, mean, and maximum values of all computed biomarkers produced with the physiological parameter sets.*

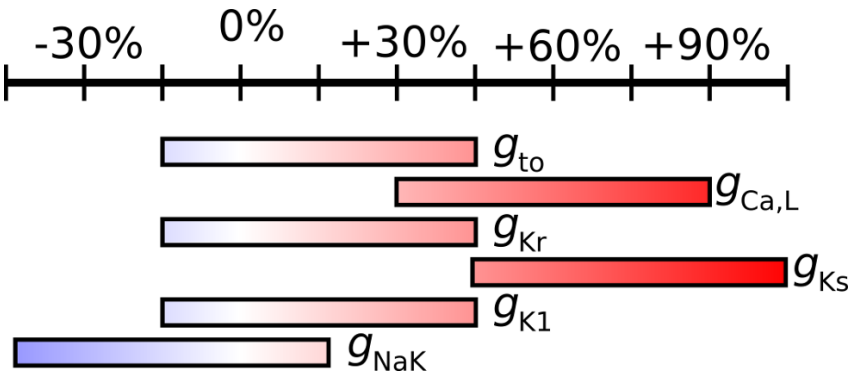

Figure 1.2: *Parameter ranges used For 'Expanded Mahajan' search.*

parameter sets matched at a CL of 600 ms, and none at a CL of 1,000ms (the increase in APD with increasing CL was disproportionately large).

In order to address the failure of the Mahajan framework in finding parameter sets that generated a physiological output with increased CL, the range of conductance variation was expanded. To determine the direction of this expansion, the first step was to increase the ranges of APD_{50} and APD_{90} by $\pm 10\%$, and the parameter space was compared to this new range. This expanded range of APD resulted in 'matches' being found at all CLs. Based on the trends in the conductances evident amongst these matches, the parameter ranges were altered and a new parameter space was explored. The new ranges are shown in Fig. 1.2, and resulted in an additional 15,625 models being simulated. However, even with this expanded search, the number of parameter sets that matched at all CLs was approximately half of that with the Shannon model.

The parameter sets producing a physiological output with the Shannon framework are shown using a dimensional stack in Fig. 1.3, along with the generated V_m and $[Ca^{2+}]_i$ profiles at a CL of 400 and 1,000 ms, and the associated distribution of conductance values. The most obvious trend is that parameter sets producing a physiological output generally had a simultaneous reduction in both $g_{Ca,L}$ and g_{K1}. This is evident in both Fig. 1.3A, demonstated by a clustering of the valid models at the bottom left of the dimensional stack, and from the associated distribution of conductances, shown in Fig. 1.3D. It also appears that the distribution of the other conductances was fairly even; however, a closer examination of the dimensional stack in Fig. 1.3A reveals trends between the parameters (demonstrating the power of the clutter-based dimension reordering technique for visualisation of multi-dimensional parameter spaces). For instance, within the g_{NaK}/g_{Kr} surfaces (Level 2 of the stack), the matching parameter sets are spread in an approximately diagonal line from top left to bottom right, indicating that when g_{NaK} was increased, this was offset by a decrease in g_{Kr}, and *vice versa*. As $g_{Ca,L}$ and g_{K1} decrease, this diagonal line moves further to the bottom left corner, indicating that a further reduction of g_{NaK} and g_{Kr} was required to continue to produce a physiological output.

The effect of g_{to} is more complicated. When $g_{Ca,L}$ and g_{K1} were reduced by 30%, and g_{NaK} was also reduced, matching parameter sets then included those with an increased g_{to}. The opposite was true when g_{NaK} was increased, as in these cases a decrease in g_{to} was necessary (square A1 in Fig. 1.3A). As g_{K1} was increased, fewer parameter sets with an increased g_{NaK} were valid, such that an increase in g_{to} was observed (squares B1, C1, and D1 in Fig. 1.3). However, in all cases where $g_{Ca,L}$ was not reduced by 30%, the opposite was true: parameter sets included reduced g_{NaK} and increased g_{to} were no longer valid (squares A2 and A3 in Fig. 1.3). Finally, in all valud parameter sets as g_{K1} was increased, g_{to} decreased. On the other hand, there appeared to be no pattern to the values of g_{Ks} within the model population.

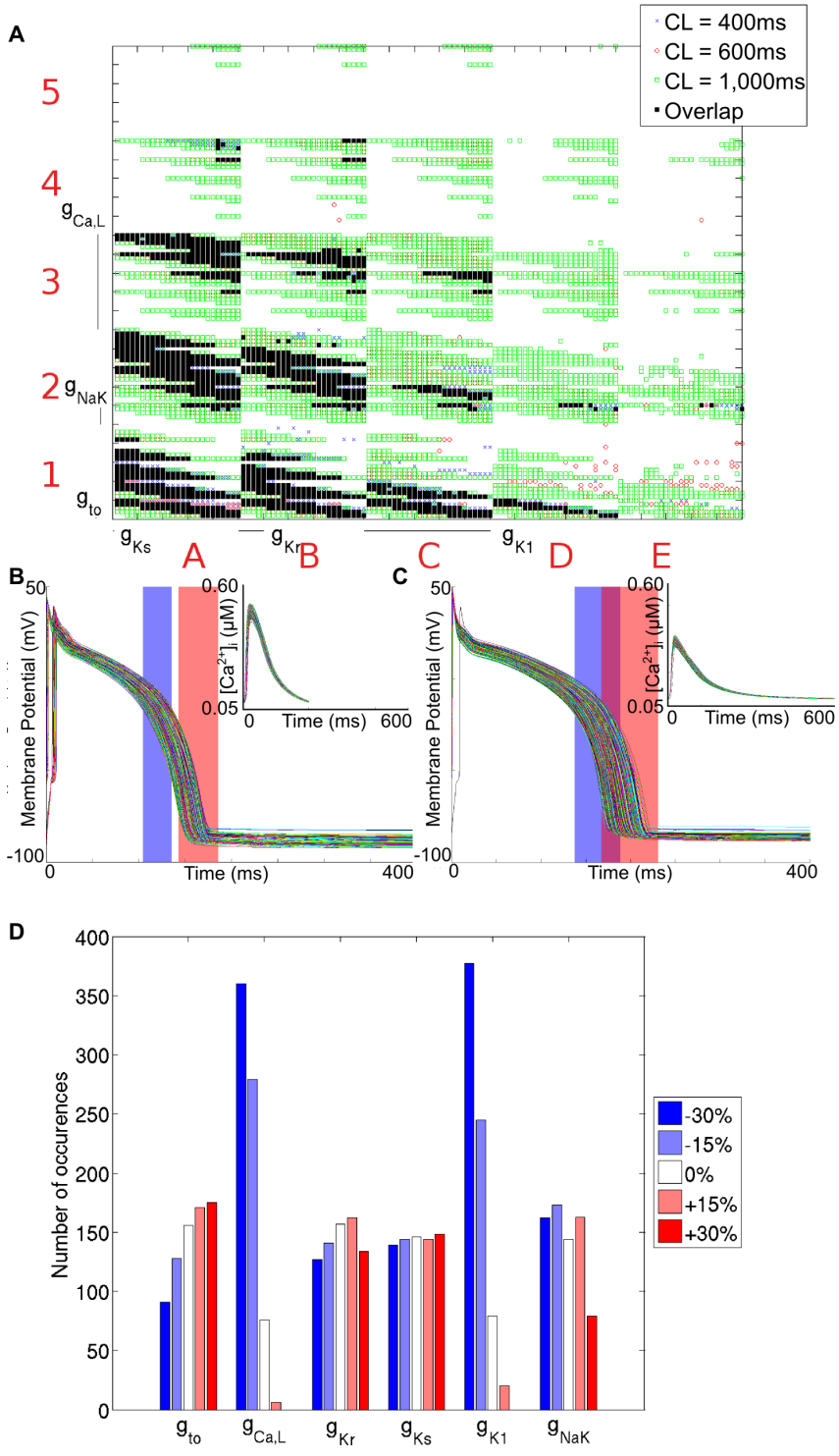

Figure 1.3: *Model population for the Shannon framework that produces values of both APD_{50} and APD_{90} that fall within the experimentally derived range. (A) Dimensional stack image showing the location of matching parameter sets for each CL and their overlap. (B) V_m and $[Ca^{2+}]_i$ (inset) profiles for the matching parameter sets at a CL of 400 ms. (C) V_m and $[Ca^{2+}]_i$ (inset) profiles for the matching parameter sets at a CL of 1,000 ms. (D) Distribution of conductance values for the valid parameter sets. For both (B) and (C), the physiological ranges of APD_{50} and APD_{90} are represented by the blue and red rectangles, respectively.*

For the expanded Mahajan search, the parameter sets producing a physiological output, the generated cellular profiles, and the distribution of valid conductance values are shown in Fig. 1.4. There are some differences compared to the Shannon framework. For instance, with the Shannon framework, g_{Ks} appeared to have no effect in determining the validity of parameter sets, while with the Mahajan framework it had a strong influence, as most matching parameter sets included the largest conductance variation ($+105\%$). The opposite was true for g_{K1}: while it had a large influence with the Shannon framework, it was relatively unimportant with the Mahajan framework. Similarly, with the Shannon framework, g_{to} and g_{NaK} generally varied in the opposite direction, while with the Mahajan framework they changed in the same direction.

With the Mahajan model, there was also a strong correlation between g_{NaK} and g_{Ks}, such that when g_{NaK} was increased, g_{Ks} also increased (demonstrated by a shift of mathcing parameter sets from the predominantly lower left corner to the upper right corner of the level two plots in Fig. 1.4A; for instance, compare the distribution within E1 and E3). On the other hand, there appeared to be no limitations on the values of g_{Kr}.

It is of note that the original model for both frameworks is not included in the final model populations. This does not in any way remove the validity of these models—they are entirely valid for the CLs for which they were designed. It can also be compared to Sato et al. (2009), in which different parameters had to be used within the model to generate the required behaviour. However, this does demonstrate the limitations of any given model, and the requirement to be careful of any applications for which the model/framework was not explicitly designed. On a related note, it can be observed that there is little variation observed in V_{rest} in both populations. While this is almost to be expected (none of the varied parameters would be expected to have a great effect on this biomarker), it should be noted that, in experimental data, V_{rest} is rarely so well-behaved.

While the results presented here suggest that variation in current conductances over a wide range of values may account for normal variability in rabbit ventricular AP repolarisation, other factors may be involved. One of the underlying assumptions of this thesis is that AP variability is primarily a result of differences in the relative magnitude of the currents, rather than underlying current dynamics, which were not varied. Changes in channel properties other than conductance could result in similar changes in AP biomarkers, and also account for some of the experimentally observed variability. Romero et al. (2011) presented a one-dimensional sensitivity analysis of the rabbit-specific frameworks used in this thesis with a similar range of parameter variation, and showed that along with repolarisation currents, APD was significantly modified by changes in the activation and inactivation rates of the associated channels. At the same time, further constraints to the model populations (*e.g.* matching of rate-adaptation of restitution properties), as well as consideration of additional biomarkers (for instance, relating to intracellular ion concentration), may be necessary to ensure their applicability to additional physiological states. This has been recently demonstrated in Walmsley et al. (2013), in which populations of failing and non-failing human ventricular myocytes with variation in current conductances were compared using various biomarkers at numerous CLs to investigate which currents drive variability in the two cell populations. Finally, as the range and resolution of parameter space sampling in teh present study was limited by computational tractability, there may be additional influences and interactions of current conductances important for ventricular AP variability that were not appreciated. As mentioned earlier, it is difficulat to properly asses the true physiological ranges of the current conductances considered in this study, so that they may be related to the values included in the calibrated populations of models. We initially varied all conductances by $\pm 30\%$, yet it was necessary with the Mahajan framework to expand this range to generate a physiological output.

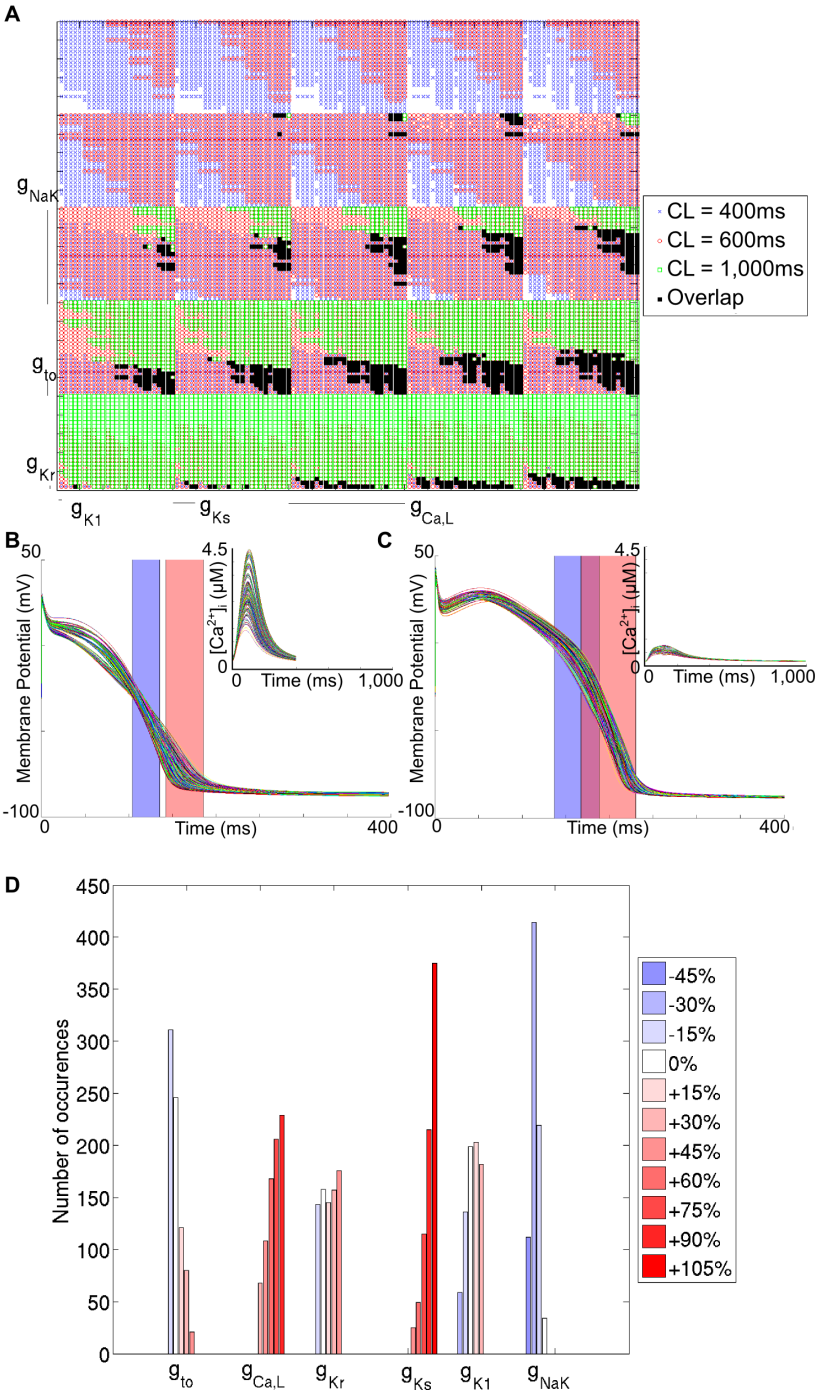

Figure 1.4: *Model population for the expanded Mahajan framework that produces values of both APD_{50} and APD_{90} that fall within the experimentally derived range. (A) Dimensional stack image showing the location of matching parameter sets for each CL and their overlap. (B) V_m and $[Ca^{2+}]_i$ (inset) profiles for the matching parameter sets at a CL of 400 ms. (C) V_m and $[Ca^{2+}]_i$ (inset) profiles for the matching parameter sets at a CL of 1,000 ms. (D) Distribution of conductance values for the valid parameter sets. For both (B) and (C), the physiological ranges of APD_{50} and APD_{90} are represented by the blue and red rectangles, respectively.*

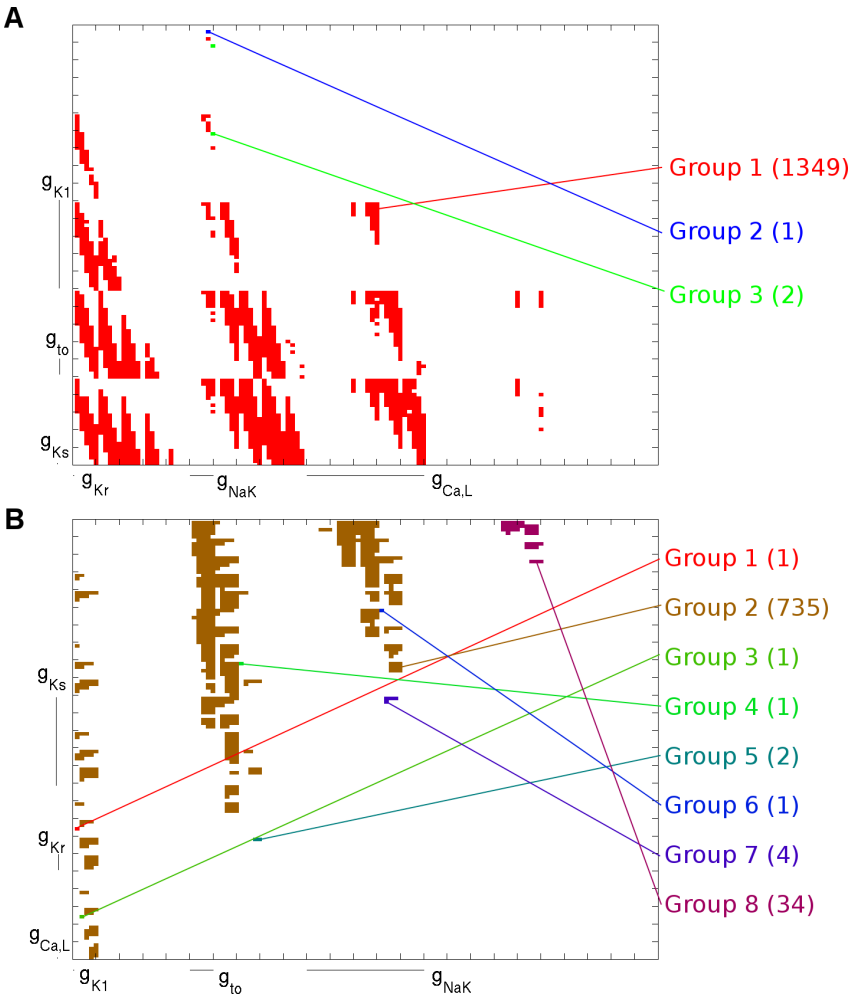

Figure 1.5: *Dimensional stack images showing connectivity within model populations for the Shannon (A) and Mahajan (B) frameworks, with a space defined as being connected if two points are connected only if they are one step away from each other in a single dimension.*

Other computational studies have used a larger range of conductances than presented here (Sobie, 2009; Britton et al., 2013; Davies et al., 2012), possibly representing the true physiological range of values, and supporting the expanded range used with the Mahajan framework..

1.4.2 Connectivity within the Parameter Space

Of note is the question which has been touched upon earlier, both in this study and others: are the populations generated here 'connected', by which it is asked whether or not one can connect all models in the population with a single parameter space, or does the population consist of several separate populations within the population space. The answer to this is irritatingly dependent on how, exactly, one defines 'connected'. If one requries connection only by one step in multiple dimensions, then the populations derived here are connected. However, if one adopts a stricter definition of connection (two models are connected only if they are one step away from each other in a single dimension), then the populations are not connected—this is shown in a dimensional stack in Fig. 1.5.

It is beyond the scope of this thesis to determine whether the two definitions of connectivity can be

Framework	Biomarker	CL (ms)	Optimum Stack Order (x, y) Low Order $\longrightarrow$ High Order		
Shannon	APD_{50}	400	(g_{to}, g_{Ks})	(g_{NaK}, g_{Kr})	$(g_{Ca,L}, g_{K1})$
		1,000	(g_{K1}, g_{Ks})	(g_{NaK}, g_{Kr})	$(g_{Ca,L}, g_{to})$
	APD_{90}	400	(g_{to}, g_{Ks})	(g_{NaK}, g_{Kr})	$(g_{Ca,L}, g_{K1})$
		1,000	(g_{K1}, g_{Ks})	(g_{NaK}, g_{Kr})	$(g_{Ca,L}, g_{to})$
	CaT	400	(g_{K1}, g_{Ks})	(g_{NaK}, g_{to})	$(g_{Ca,L}, g_{Kr})$
		1,000	(g_{K1}, g_{Ks})	(g_{NaK}, g_{Kr})	$(g_{Ca,L}, g_{to})$
Mahajan	APD_{50}	400	(g_{Kr}, g_{K1})	$(g_{Ks}, g_{Ca,L})$	(g_{to}, g_{NaK})
		1,000	(g_{Kr}, g_{K1})	$(g_{to}, g_{Ca,L})$	(g_{Ks}, g_{NaK})
	APD_{90}	400	$(g_{Kr}, g_{Ca,L})$	(g_{K1}, g_{Ks})	(g_{to}, g_{NaK})
		1,000	(g_{Kr}, g_{K1})	(g_{Ks}, g_{to})	$(g_{Ca,L}, g_{NaK})$
	CaT	400	(g_{Kr}, g_{K1})	(g_{to}, g_{Ks})	$(g_{NaK}, g_{Ca,L})$
		1,000	(g_{Kr}, g_{K1})	(g_{Ks}, g_{to})	$(g_{NaK}, g_{Ca,L})$

Table 1.4: *Optimum stack order for APD_{50}, APD_{90}, and CaT for the Shannon and Mahajan frameworks, at CLs of 400 and 1,000 ms. Each pair of parameters represents low, medium, or high order current conductances. For each pair, the first component is plotted on the x-axis and the second component on the y-axis. The (x, y) order can be reversed without affecting the result, though only if* all (x, y) *pairs are reversed.*

reconciled—whether by increased resolution, or by inclusion of alternative parameters, those semi-connected regions will become connected. However, if we work on the (somewhat reasonable) assumption that either they can, or the looser defintion of connectivity is a reasonable approximation, this has significant implications for population construction, in that it implies that, once a 'valid' model has been found, the search for other 'valid' models can be directed, and thus the computational task of searching the entire parameter space is reduced.

1.5 Effects of Parameter Variation

Using the biomarkers thus defined as providing measures of goodness-of-fit, it is now possible to assess the effects of parameter variation on the model populations; it also allows judgement of how these different biomarkers are affected by these different parameters, and how these differences are altered based on CL. The dimensional stack images showing these effects are presented in Fig. 1.6 (for the Shannon population) and Fig. ?? (for the Mahajan population). In addition, the optimum stack orders are shown in Table 1.4.

These results demonstrate how the relative importance of the varied current conductances was dependent on both the CL, and on the biomarker being considered. In considering this, it should be noted that the non-linear interactions between currents and ion concentrations often resulted in different changes in the current magnitudes that might be expected from the change in current conductance. For instance, when g_{Ks} was subject to $\pm 30\%$ variation at a CL of 1,000 ms, the amplitude of I_{Ks} varied from -99% to $+386\%$ for the Mahajan population. (TODO: CHECK THE DETAILS OF THIS MORE PRECISELY).

The optimum stack order, which is an indication of both the relative importance of the individual conductances on the biomarker and the inter-relation between parameters, changes with CL. The extent of this change is unpredictable, and can be dramatic. This is best demonstrated with the Shan-

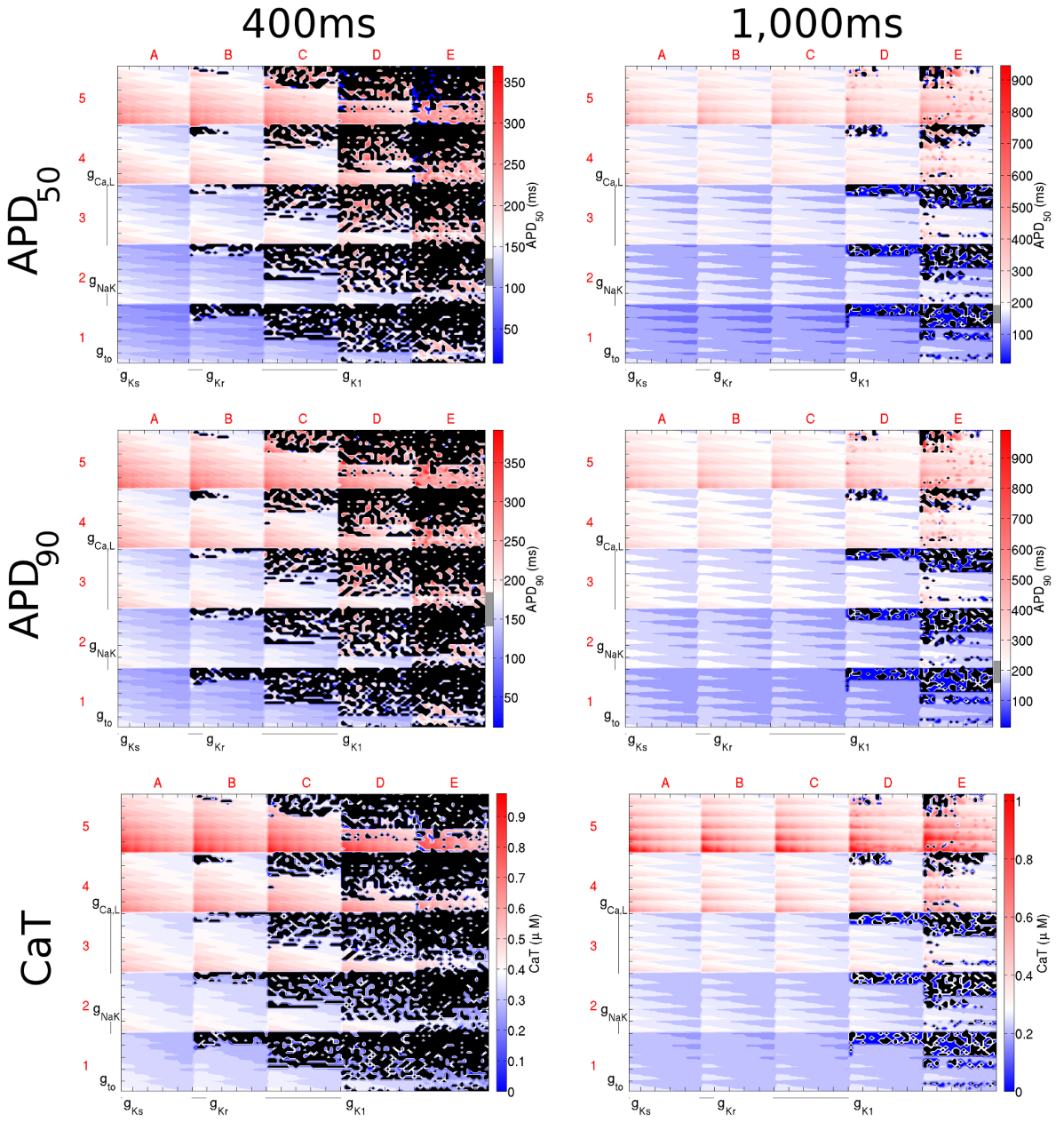

Figure 1.6: *Dimensional stack images demonstrating the effect of simultaneously varying the magnitude of six repolarising current conductances in the Shannon model. The top, middle, and bottom rows show the effects on APD_{50}, APD_{90}, and CaT, respectively. The left column is based on simulations with a CL of 400 ms and the right with a CL of 1,000 ms. In the contour plots, red represents an increase from the initial parameter value, blue a decrease, and white no change. The physiological range determined from the literature (see §1.4 for details) is represented by the grey region next to the colour bars in each panel. Black dots represent parameter sets with which the model did not reach steady state. In this case the optimum stack orders are not displayed; instead the order before optimisation has been used, which allowed direct comparison of the stacks to reveal differences in effects on each biomarker.*

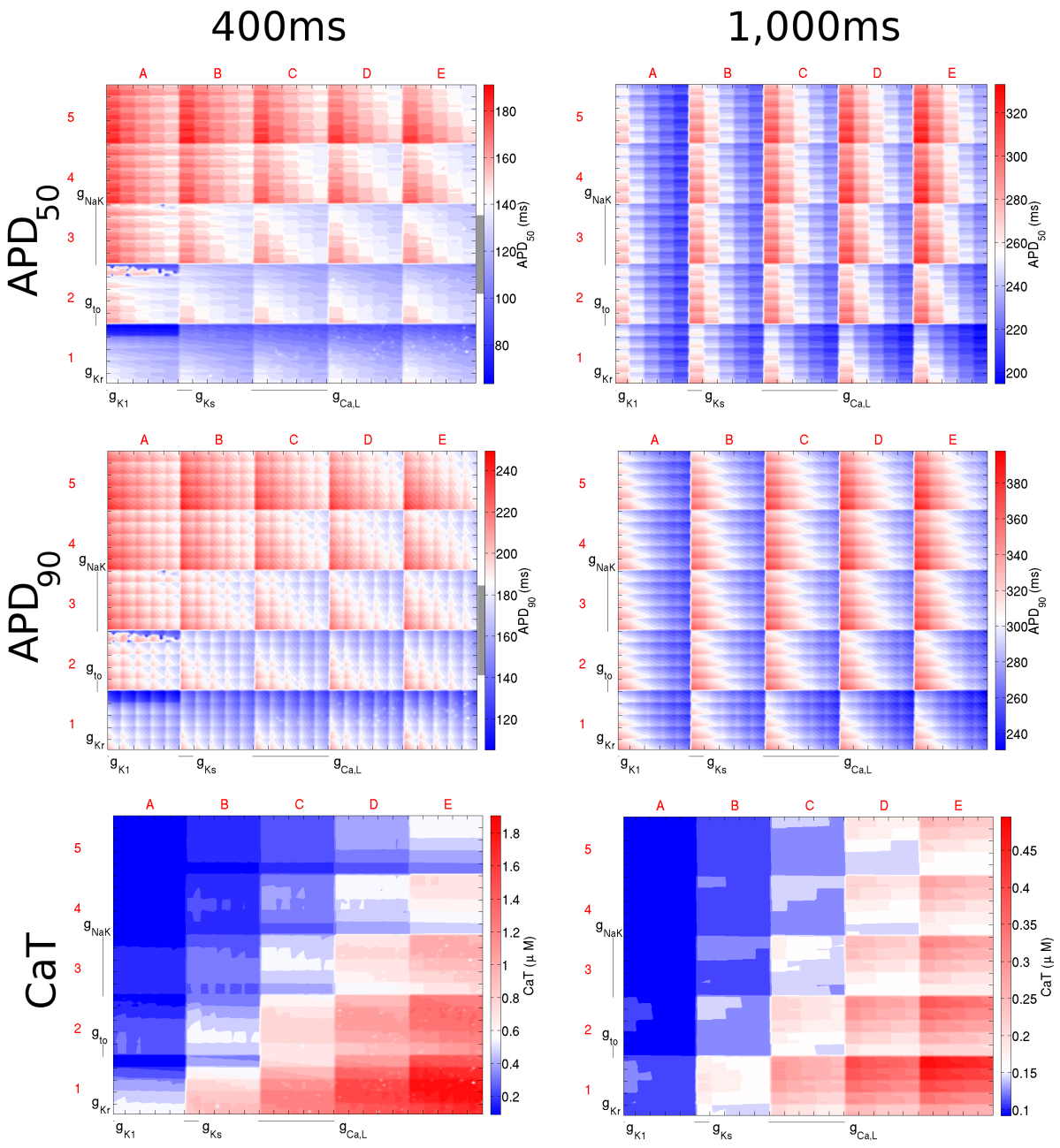

Figure 1.7: *Dimensional stack images demonstrating the effect of simultaneously varying the magnitude of six repolarising current conductances in the Mahajan model. The top, middle, and bottom rows show the effects on APD_{50}, APD_{90}, and CaT, respectively. The left column is based on simulations with a CL of 400 ms and the right with a CL of 1,000 ms. In the contour plots, red represents an increase from the initial parameter value, blue a decrease, and white no change. The physiological range determined from the literature for a CL of 400 ms is represented by the grey region next to the colour bars in each panel (the grey region is absent for a CL of 1,000 ms as the APD values fell outside of the physiological range). In this case the optimum stack orders are not displayed; instead the order before optimisation has been used, which allows direct comparison of the stacks to reveal differences in effects on each biomarker.*

non framework, and the change in influence of g_{to} on APD_{50} and APD_{90}. At a Cl of 400 ms, g_{to} was a low-order conductance (reflecting a low importance), while at a CL of 1,000 ms, it became a high-order conductance. The relative importance of g_{K1} decreases at the same time. However, this degree of change does not always occur—$g_{Ca,L}$ was consistently of high-order and g_{Ks} of low-order, while g_{Kr} and g_{NaK} were generally of medium-order.

For the Mahajan framework, as CL increased, the relative importance of g_{to} decreased. This is opposite to the response seen with the Shannon framework. At the same time, g_{Ks} becomes more influential, despite little change in its position in the optimum stack order. This can be seen by examining the difference between the dimensional stacks with CLs of 400 and 1,000 ms shown in Fig. 1.7. At a CL of 400 ms, the greatest effect on APD (represented by deep red and blue) is seen at the edges of the dimensional stack image (squares A1, A5, E1 and E5), indicating an extreme increase/decrease in $g_{Ca,L}$ and g_{NaK} is required for such effects. However, with an increase in CL, the maximum effect of the change in seen throughout the dimensional stack image, as a result of the increased importance of g_{Ks}. In contrast, the relative importance of g_{NaK} and g_{Kr} were independent of CL, being consistently one of the highest and lowest order conductances, respectively.

The same optimum stack order is rarely shared between APD_{50}/APD_{90} and CaT; moreover, there are instances where even the APD biomarkers have different optimum stack orders (see the Mahajan framework results). This point becomes more evident with inspection of the dimensional stack images—the distribution of changes is drastically different between AP and $[Ca^{2+}]_i$ biomarkers, and subtly different between the AP biomarkers themselves. This emphasises the folly, already noted elsewhere (Walmsley et al., 2013), of the thinking of 'parameter X' is very influential. Rather, the conditions under which parameter X is important, and by which metric it is important, must always be added as caveats to such sweeping statements.

These results can be contrasted with the results presented in Heijman et al. (2013), which indicated I_{Na} and I_{Kr} as the most influential for affecting BVR. While the obvious differences between these studies, both in terms of methods and in terms of goals, should be remembered, it is instructive to note the common themes, and the implications of these works on the current results. For example, Heijman *et al.* demonstrated little stochastic effects of pumps and exchangers due to their low throughput and high expression rate 'smoothing out' stochastic effects. This is compared the results presented here, and in the work from Sobie *et al.*, which noted the effect of I_{NaK} and I_{NaCa}—while they may be noted as having little stochastic effect, their interactions with other components reinforces their importance in their own right. Furthermore, it is implied that their effects are mediated via their effect on ion concentrations and the like rather than direct effect on the AP, as these do not affect BVR directly.

The results presented in this section serve as an illustration of the importance of considering (1) the independence of the relative importance of parameters on the different biomarkers, and (2) the effect of CL when determining the effects of current conductance variability on biomarkers. It is also worth noting the differences that exist between the two frameworks when subjected to identical degrees of parameter variation, with the consideration that the Mahajan framework is based in large part on the Shannon framework. However, the non-linear nature of the interactions between the components that make up a biophysically detailed cell model mean that, even with these common elements, the response can be drastically different.

1.6 Rate Dependence of Biomarkers

Related to the changes in parameter importance varying with rate is variability of the biomarker distribution itself with changes in CL. Histograms showing the variability of APD_{50}, APD_{90} and CaT across all combinations of current conductances are shown in Fig. 1.8. Both frameworks demonstrated similar distributions for both APD_{50} and APD_{90} (upper and middle panels). They differed, however, in that the Mahajan framework demonstrated more narrow distributions than the Shannon framework, while the Shannon framework generated more APD values that fell within the physiological range (discussed in §1.4.1). For the Shannon framework, the shape of the APD_{50} and APD_{90} distributions were relatively well conserved between a CL of 400 and 1,000 ms, other than an increase in the number of matching parameter sets. In constrast, the Mahajan framework demonstrated a widening of the APD_{50} and APD_{90} distributions, as well as an increase in their mean. In the case of simulations with a CL of 1,000 ms, the increase in APD was such that the entire distribution fell outside of teh physiological range. The change in CaT distribution with a change in CL was more dramatic (lower panels in Fig. 1.8). For the Shannon framework, the distribution narrowed with an increase in CL. The distribution with the Mahajan framework followed a similar pattern, however with an even larger change. At a CL of 400 ms, the range of CaT was very broad ($\sim 0.1\mu$M to $\sim 1.9\mu$M), indicating that CaT was relatively poorly constrained within the parameter space. When CL was increased, however, the range was greatly reduced ($\sim 0.1\mu$M to $\sim 0.5\mu$M)

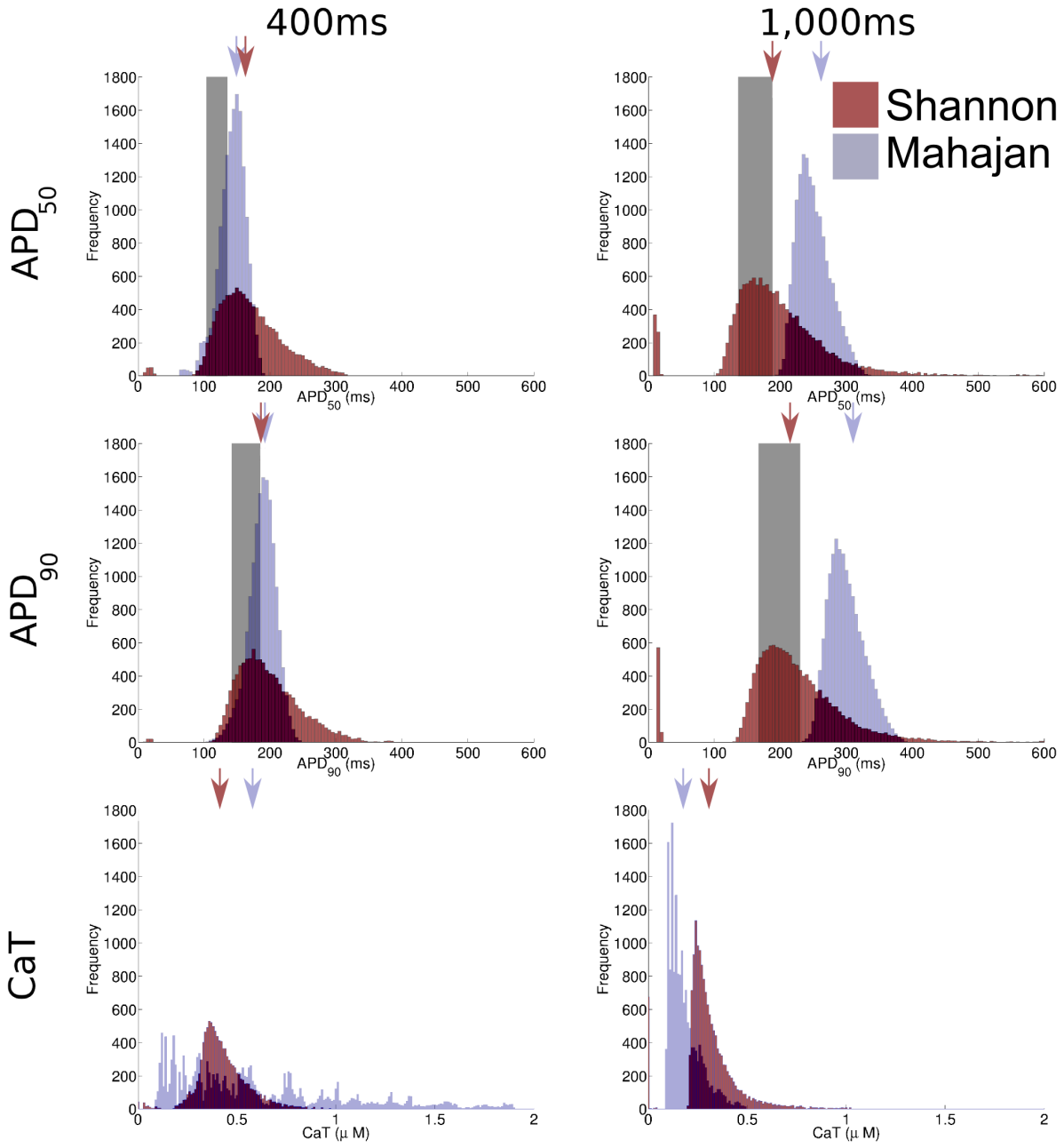

Figure 1.8: *Histograms showing the range of APD_{50}, APD_{90}, and CaT in the model populations. The value generated with the initial parameter set for each framework is indicated by the arrow. The physiological range of APD_{50} and APD_{90} derived from the literature are represented by the boxed area.*

Bibliography

Biagetti, M. O. and Quinteiro, R. A. (2006). Gender differences in electrical remodeling and susceptibility to ventricular arrhythmias in rabbits with left ventricular hypertrophy. *Heart Rhythm : the Official Journal of the Heart Rhythm Society*, 3(7):832–9.

Britton, O. J., Bueno-Orovio, A., Van Ammel, K., Lu, H. R., Towart, R., Gallacher, D. J., and Rodríguez, B. (2013). Experimentally calibrated population of models predicts and explains intersubject variability in cardiac cellular electrophysiology. *Proceedings of the National Academy of Sciences of the United States of America*.

Chen, X., Cordes, J. S., Bradley, J. A., Sun, Z., and Zhou, J. (2006). Use of arterially perfused rabbit ventricular wedge in predicting arrhythmogenic potentials of drugs. *Journal of Pharmacological and Toxicological Methods*, 54(3):261–72.

Davies, M. R., Mistry, H. B., Hussein, L., Pollard, C. E., Valentin, J.-P., Swinton, J., and Abi-Gerges, N. (2012). An in silico canine cardiac midmyocardial action potential duration model as a tool for early drug safety assessment. *American Journal of Physiology - Heart and Circulatory Physiology*, 302(7):H1466–80.

Eckardt, L., Haverkamp, W., Göttker, U., Madeja, M., Johna, R., Borggrefe, M., and Breithardt, G. (1998). Divergent effect of acute ventricular dilatation on the electrophysiologic characteristics of d,l-sotalol and flecainide in the isolated rabbit heart. *Journal of Cardiovascular Electrophysiology*, 9(4):366–83.

Fülöp, L., Bányász, T., Magyar, J., Szentandrássy, N., Varró, A., and Nánási, P. P. (2004). Reopening of L-type calcium channels in human ventricular myocytes during applied epicardial action potentials. *Acta Physiologica Scandinavica*, 180(1):39–47.

Gemmell, P., Burrage, K., Rodríguez, B., and Quinn, T. A. (2010). Exploring the parameter space of a rabbit ventricular action potential model to investigate the effect of variation on action potential and calcium transients. *Annual International Conference of the IEEE Engineering in Medicine and Biology Society*, 2010:2662–5.

Goldhaber, J. I., Xie, L.-H., Duong, T., Motter, C., Khuu, K., and Weiss, J. N. (2005). Action potential duration restitution and alternans in rabbit ventricular myocytes: the key role of intracellular calcium cycling. *Circulation Research*, 96(4):459–66.

Hashambhoy, Y. L., Winslow, R. L., and Greenstein, J. L. (2011). CaMKII-dependent activation of late INa contributes to cellular arrhythmia in a model of the cardiac myocyte. *Conference proceedings : ... Annual International Conference of the IEEE Engineering in Medicine and Biology Society. IEEE Engineering in Medicine and Biology Society. Conference*, 2011:4665–8.

Heijman, J., Zaza, A., Johnson, D. M., Rudy, Y., Peeters, R. L. M., Volders, P. G. A., and Westra,

R. L. (2013). Determinants of Beat-to-Beat Variability of Repolarization Duration in the Canine Ventricular Myocyte: A Computational Analysis. *PLoS Computational Biology*, 9(8):e1003202.

Iost, N., Virág, L., Opincariu, M., Szécsi, J., Varró, A., and Papp, J. G. (1998). Delayed rectifier potassium current in undiseased human ventricular myocytes. *Cardiovascular Research*, 40(3):508–15.

Jung, B.-C., Lee, S.-H., Cho, Y.-K., Park, H.-S., Kim, Y.-N., Lee, Y.-S., and Shin, D.-G. (2011). Role of the alternans of action potential duration and aconitine-induced arrhythmias in isolated rabbit hearts. *Journal of Korean Medical Science*, 26(12):1576–81.

Kirchhof, P., Degen, H., Franz, M. R., Eckardt, L., Fabritz, L., Milberg, P., Läer, S., Neumann, J., Breithardt, G., and Haverkamp, W. (2003). Amiodarone-induced postrepolarization refractoriness suppresses induction of ventricular fibrillation. *Journal of Pharmacology and Experimental Therapeutics*, 305(1):257–263.

Kurz, R. W., Mohabir, R., Ren, X. L., and Franz, M. R. (1993). Ischaemia induced alternans of action potential duration in the intact-heart: dependence on coronary flow, preload and cycle length. *European Heart Journal*, 14(10):1410–20.

Li, G.-R., Yang, B., Feng, J., Bosch, R. F., Carrier, M., and Nattel, S. (1999). Transmembrane ICa contributes to rate-dependent changes of action potentials in human ventricular myocytes. *American Journal of Physiology*, 276(1 Pt 2):H98–H106.

Marder, E. and Taylor, A. L. (2011). Multiple models to capture the variability in biological neurons and networks. *Nature Neuroscience*, 14(2):133–8.

McIntosh, M. A., Cobbe, S. M., and Smith, G. L. (2000). Heterogeneous changes in action potential and intracellular Ca2+ in left ventricular myocyte sub-types from rabbits with heart failure. *Cardiovascular Research*, 45(2):397–409.

Mirams, G. R., Arthurs, C. J., Bernabeu, M. O., Bordas, R., Cooper, J., Corrias, A., Davit, Y., Dunn, S.-J., Fletcher, A. G., Harvey, D. G., Marsh, M. E., Osborne, J. M., Pathmanathan, P., Pitt-Francis, J., Southern, J., Zemzemi, N., and Gavaghan, D. J. (2013). Chaste: an open source C++ library for computational physiology and biology. *PLoS Computational Biology*, 9(3):e1002970.

Noble, D. and Rudy, Y. (2001). Models of cardiac ventricular action potentials: iterative interaction between experiment and simulation. *Philosophical Transactions of the Royal Society A: Mathematical, Physical and Engineering Sciences*, 359(1783):1127–1142.

Pueyo, E., Corrias, A., Virág, L., Jost, N., Szél, T., Varró, A., Szentandrássy, N., Nánási, P. P., Burrage, K., and Rodríguez, B. (2011). A multiscale investigation of repolarization variability and its role in cardiac arrhythmogenesis. *Biophysical Journal*, 101(12):2892–902.

Quinn, T. A., Granite, S., Allessie, M. A., Antzelevitch, C., Bollensdorff, C., Bub, G., Burton, R. A. B., Cerbai, E., Chen, P.-S., Delmar, M., DiFrancesco, D., Earm, Y. E., Efimov, I. R., Egger, M., Entcheva, E., Fink, M., Fischmeister, R., Franz, M. R., Garny, A., Giles, W. R., Hannes, T., Harding, S. E., Hunter, P. J., Iribe, G., Jalife, J., Johnson, C. R., Kass, R. S., Kodama, I., Koren, G., Lord, P., Markhasin, V. S., Matsuoka, S., McCulloch, A. D., Mirams, G. R., Morley, G. E., Nattel, S., Noble, D., Olesen, S. P., Panfilov, A. V., Trayanova, N. A., Ravens, U., Richard, S., Rosenbaum, D. S., Rudy, Y., Sachs, F., Sachse, F. B., Saint, D. A., Schotten, U., Solovyova, O., Taggart, P., Tung, L., Varró, A., Volders, P. G. A., Wang, K., Weiss, J. N., Wettwer, E., White, E., Wilders, R., Winslow, R. L., and Kohl, P. (2011). Minimum Information about a Cardiac Electrophysiology

Experiment (MICEE): standardised reporting for model reproducibility, interoperability, and data sharing. *Progress in Biophysics and Molecular Biology*, 107(1):4–10.

Quinn, T. A. and Kohl, P. (2013). Combining wet and dry research: experience with model development for cardiac mechano-electric structure-function studies. *Cardiovascular Research*, 97(4):601–11.

Romero, L., Carbonell, B., Trénor, B., Rodríguez, B., Sáiz, J., and Ferrero, J. M. (2011). Systematic characterization of the ionic basis of rabbit cellular electrophysiology using two ventricular models. *Progress in Biophysics and Molecular Biology*, 107(1):60–73.

Romero, L., Pueyo, E., Fink, M., and Rodríguez, B. (2009). Impact of ionic current variability on human ventricular cellular electrophysiology. *American Journal of Physiology - Heart and Circulatory Physiology*, 297(4):H1436–45.

Sarkar, A. X. and Sobie, E. A. (2010). Regression analysis for constraining free parameters in electrophysiological models of cardiac cells. *PLoS Computational Biology*, 6(9):e1000914.

Sarkar, A. X. and Sobie, E. A. (2011). Quantification of repolarization reserve to understand interpatient variability in the response to proarrhythmic drugs: a computational analysis. *Heart Rhythm : the Official Journal of the Heart Rhythm Society*, 8(11):1749–55.

Sato, D., Xie, L.-H., Sovari, A. A., Tran, D. X., Morita, N., Xie, F., Karagueuzian, H., Garfinkel, A., Weiss, J. N., and Qu, Z. (2009). Synchronization of chaotic early afterdepolarizations in the genesis of cardiac arrhythmias. *Proceedings of the National Academy of Sciences of the United States of America*, 106(9):2983–8.

Sims, C., Reisenweber, S., Viswanathan, P. C., Choi, B.-R., Walker, W. H., and Salama, G. (2008). Sex, age, and regional differences in L-type calcium current are important determinants of arrhythmia phenotype in rabbit hearts with drug-induced long QT type 2. *Circulation Research*, 102(9):e86–100.

Sobie, E. A. (2009). Parameter sensitivity analysis in electrophysiological models using multivariable regression. *Biophysical Journal*, 96(4):1264–74.

Sobie, E. A. and Sarkar, A. X. (2011). Regression methods for parameter sensitivity analysis: applications to cardiac arrhythmia mechanisms. In *Annual International Conference of the IEEE Engineering in Medicine and Biology Society*, volume 2011, pages 4657–60.

Syed, Z., Vigmond, E., Nattel, S., and Leon, L. J. (2005). Atrial cell action potential parameter fitting using genetic algorithms. *Medical & Biological Engineering & Computing*, 43(5):561–71.

Szentandrássy, N., Banyasz, T., Biro, T., Szabo, G., Toth, B. I., Magyar, J., Lazar, J., Varró, A., Kovacs, L., and Nanasi, P. P. (2005). Apico-basal inhomogeneity in distribution of ion channels in canine and human ventricular myocardium. *Cardiovascular Research*, 65(4):851–60.

Szigligeti, P., Pankucsi, C., Bányász, T., Varró, A., and Nánási, P. P. (1996). Action potential duration and force-frequency relationship in isolated rabbit, guinea pig and rat cardiac muscle. *Journal of Comparative Physiology. B, Biochemical, Systemic, and Environmental Physiology*, 166(2):150–5.

Tanskanen, A. J., Greenstein, J. L., O'Rourke, B., and Winslow, R. L. (2005). The role of stochastic and modal gating of cardiac L-type Ca2+ channels on early after-depolarizations. *Biophysical Journal*, 88(1):85–95.

Verkerk, A. O., Wilders, R., Veldkamp, M. W., de Geringel, W., Kirkels, J. H., and Tan, H. L. (2005). Gender disparities in cardiac cellular electrophysiology and arrhythmia susceptibility in human failing ventricular myocytes. *International Heart Journal*, 46(6):1105–18.

Walmsley, J., Mirams, G. R., Bahoshy, M., Bollensdorff, C., Rodríguez, B., and Burrage, K. (2010). Phenomenological modeling of cell-to-cell and beat-to-beat variability in isolated Guinea Pig ventricular myocytes. In *Annual International Conference of the IEEE Engineering in Medicine and Biology Society*, volume 2010, pages 1457–60.

Walmsley, J., Rodríguez, J. F., Mirams, G. R., Burrage, K., Efimov, I. R., and Rodríguez, B. (2013). mRNA Expression Levels in Failing Human Hearts Predict Cellular Electrophysiological Remodeling: A Population-Based Simulation Study. *PloS One*, 8(2):e56359.

Wu, L., Ma, J., Li, H., Wang, C., Grandi, E., Zhang, P., Luo, A., Bers, D. M., Shryock, J. C., and Belardinelli, L. (2011). Late sodium current contributes to the reverse rate-dependent effect of IKr inhibition on ventricular repolarization. *Circulation*, 123(16):1713–20.

Yan, G.-X., Rials, S. J., Wu, Y., Liu, T., Xu, X., Marinchak, R. A., and Kowey, P. R. (2001). Ventricular hypertrophy amplifies transmural repolarization dispersion and induces early afterdepolarization. *American Journal of Physiology - Heart and Circulatory Physiology*, 281:H1968–H1975.